Applied Surface Science 257 (2011) 2955–2959

Contents lists available at ScienceDirect

Applied Surface Science

journal homepage: www.elsevier.com/locate/apsusc

Preparation and properties of ZnS superhydrophobic surface with hierarchical structure

Lujun Yao [a], Maojun Zheng [a,*], Shuanghu He [a], Li Ma [b], Mei Li [b], Wenzhong Shen [a]

[a] Laboratory of Condensed Matter Spectroscopy and Opto-Electronic Physics, and Key Laboratory of Artificial Structures and Quantum Control (Ministry of Education), Department of Physics, Shanghai Jiao Tong University, Shanghai 200240, People's Republic of China
[b] School of Chemistry & Chemical Technology, Shanghai Jiao Tong University, Shanghai 200240, People's Republic of China

ARTICLE INFO

Article history:
Received 19 August 2010
Received in revised form 21 October 2010
Accepted 21 October 2010
Available online 27 October 2010

Key words:
Novel ZnS nanostructure
Chemical vapor deposition
Self-cleaning
Super water-repellent
Electrowetting

ABSTRACT

A novel ZnS hierarchical structure composed of nanorod arrays with branched nanosheets and nanowires grown on their upside walls, was synthesized over Au-coated silicon substrate via chemical vapor deposition technique. Contact angle and sliding angle of this hierarchical film with no surface modification were measured to be about 153.8° and 9.1° for 5 μl water droplets. Self-cleaning behavior and dynamic water-repelling performance were clearly demonstrated. In addition, electrowetting transition phenomenon from superhydrophobic to hydrophilic state happened when a critical bias ~7.0 V was applied. Below this threshold voltage, the contact angle change is little. This work for the first time reports the creation of ZnS superhydrophobic surface and could enrich its research field as surface functional materials.

1. Introduction

There are vast singular morphologies on biological surfaces in both the plant and animal kingdom that exhibit super-water-repellent properties, many intriguing examples are provided by the sacred lotus or rice leaves, wings of cicada and water strider's legs [1–4], which have attracted tremendous scientific interest. A combination of surface roughness at both the micro- and nanoscale with a low surface energy of the materials has been considered as the key factors to superhydrophobicity. Many research efforts were made towards the creation of artificial water-repellent nanomaterials, and it became an attractive goal in some industrial fields for the removal of undesirable contaminants from the surfaces of high-quality products. However, the capacity to control surface wettability is also a highly desirable attribute in order to their wide usage range of chemical, biological and electronic applications, so it is indispensable to develop smart surfaces that are able to undergo fast wettability changes. These changes cannot be converted by the intrinsic properties of the liquid and should require external inducement for surface wettability response such as light irradiation [5,6], pH [7], electric field [8,9], heating [10] and solvent treatment [11]. The electric field across the liquid–solid interface will lower the surface tension and cause electrowetting, which has already been used for microfluidic switches, display technology, and lab-on-chip systems.

Recently, various semiconductor nanomaterials involving carbon nanotubes, silicon nanowires, ZnO and TiO_2 nanostructures [12–15], have been studied on their superhydrophobic properties by the help of low energy coating materials. As an important II–VI semiconductor with wide bandgap of 3.7 eV at room temperature, ZnS has been widely used in a great variety of applications such as electroluminescence, field emitters and photocatalysis. Kinds of ZnS nanostructures including rod, wire, belt, cable, tetrapod as well as cone-like morphologies [16–19] have been synthesized in the past. However, there are no reports on the preparation of superhydrophobic ZnS surfaces to date. In this paper, we presented the synthesis of a hierarchical ZnS structure consisting of nanorod arrays with branched nanostructures grown on their upside walls via chemical vapor deposition technique. We demonstrated the self-cleaning behavior, the dynamic water-repellent phenomenon and electrowetting of this hierarchical film. It is the first time to study wettability of ZnS nanomaterials and could arouse much interest in extending its applications.

2. Experimental

2.1. Fabrication of ZnS architecture

In a typical experiment, a one-end open quartz tube connected to a rotary vacuum pump and an Ar gas inlet through a vacuum

* Corresponding author. Tel.: +86 021 54743242; fax: +86 021 54741040.
E-mail address: mjzheng@sjtu.edu.cn (M. Zheng).

0169-4332/$ – see front matter © 2010 Elsevier B.V. All rights reserved.
doi:10.1016/j.apsusc.2010.10.098

coupling, was used for the synthesis. The n-type silicon wafer used as the substrate was sonicated in acetone, dried with nitrogen and then was sputterred with a thin layer (~25 Å) of Au film. Commercially available high purity Zn powder, sulfur powder and graphite powder with a molar ratio of 1:2.5:1 was used as source materials. The additive graphite powder can relax the thermal evaporation rate and make the carbothermal reduction of ZnS which could generate on the surface of source materials and would not beneficial to the thermal evaporation of Zn and S powders during the growth process. A ceramic boat containing 2 g mixture powder was loaded at the centre of the quartz tube furnace, the distance between silicon substrate and reagent powder was about 6 cm. The tube furnace was firstly evacuated for 1 h, then Ar was used as carrier gas at a flow rate of 50 sccm to facilitate the reaction. The furnace temperature was raised to 750 °C quickly and held for 30 min. After the system was cooled naturally, light gray product was deposited on n-type silicon substrate.

2.2. Characterization and properties

The morphology of the as-synthesized ZnS products was examined by field emission scanning electron microscopy (FE-SEM, Philips Sirion 200) and X-ray diffraction (Bruker-AXS system). The Raman spectrum was recorded at room temperature by a Jobin Yvon LabRAM HR 800UV micro-Raman system with system under an Ar^+ (5145 Å) laser excitation. Contact angle (CA) and sliding angle (SA) were measured using an optical contact-angle meter system (Data Physics Instrument GmbH, Germany) at ambient temperature. The static CA values were the averages of three independent points.

3. Results and discussion

Fig. 1(a) shows the cross-sectional image of the as-synthesized ZnS product, it is characterized by well-aligned nanorod arrays and some detailed nanostructures on the tops, the average diameter and length of the nanorods are around 800 nm and 15 μm. Fig. 1(b) reveals that nanostructures of the top layer is totally different, and it mainly consists of nanosheets and slender nanowires. Most of these nanowires are less than 20 nm in diameter, they tangled with each other to form a reticular structure. Fig. 1(c) and (d) is the typical top-view and tilted SEM images of an individual nanorod with branched nanostructures in high-magnification, respectively. It was confirmed that these branched nanosheets and nanowires were mainly grown form the upside walls of the arrayed nanorods, which could be considered as a hierarchical structure.

Fig. 2(a) is the energy-dispersive X-ray (EDX) spectroscopy recorded on a selected area of the ZnS architecture, indicating that it is composed of Zn and S only (Zn:S = 51.93:48.07) and has 1:1 Zn/S composition within experimental error. Here we mainly considered the stoichiometric ratio of Zn and S elements, so we did not regard the Au element and removed it from the EDX spectroscopy. Fig. 2(b) presents the X-ray diffraction, all reflected peaks with preferred orientation (0 0 2) can be indexed to the hexagonal wurtzite structure of ZnS with lattice parameters a = 3.80 Å and c = 6.23 Å, in good agreement with the Joint Committee on Powder Diffraction Standards (JCPDS) 75-1534 database. We suggest that the growth of nanorod arrays follows the vapor–liquid–solid (VLS) [20] mode. Zn vapor and S vapor were rapidly generated at the centre of the quartz tube furnace at high temperature, transported by the carrier gas and diffused into Au nanodroplets to form Au–ZnS nanocomposite particles. On supersaturation, the well-aligned ZnS nanorod in large

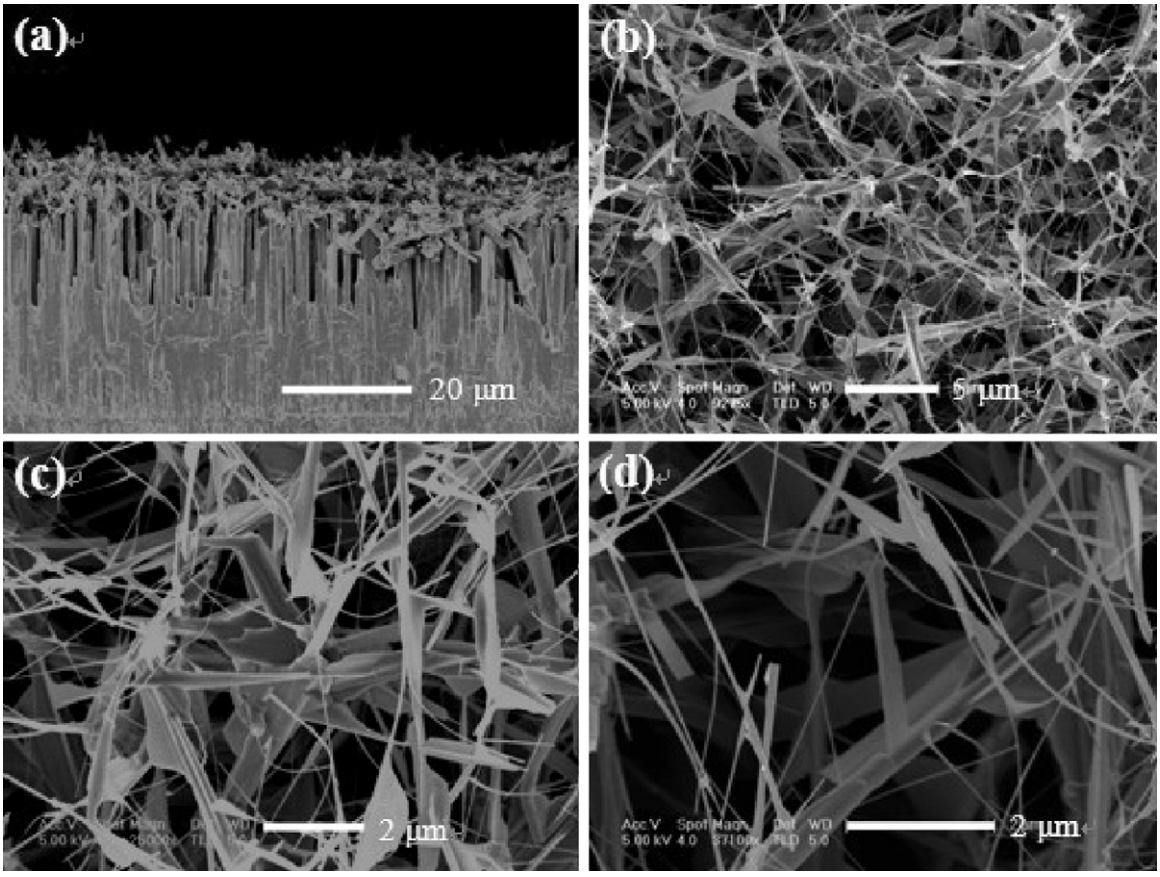

Fig. 1. (a) The cross-sectional and (b) top-view FE-SEM images of the deposited ZnS product. (c and d) High-magnification images showing the branched nanostructures.

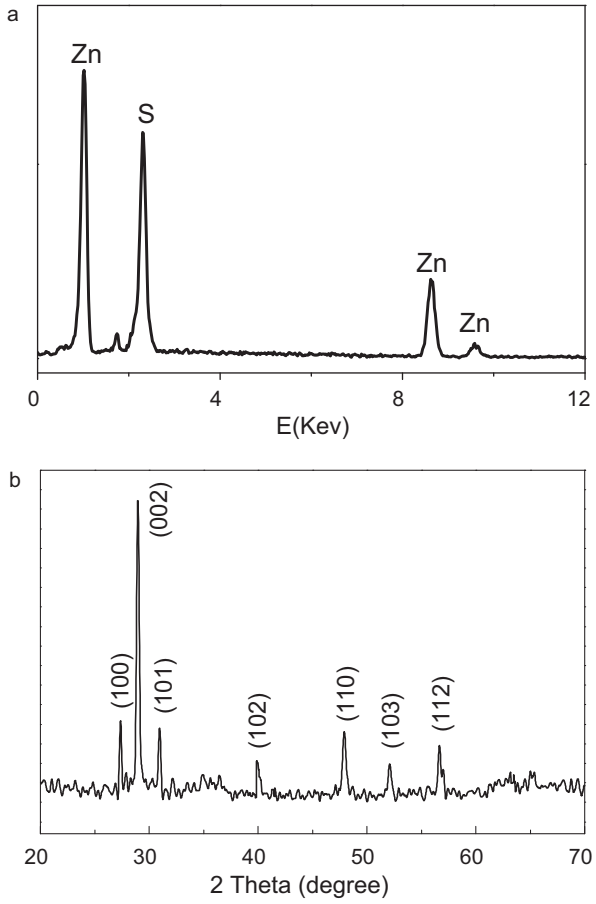

Fig. 2. (a) EDX spectroscopy recorded on a selected area and (b) XRD pattern of the ZnS product.

diameter were deposited. However, with the reaction processing, sulfur source became less due to its low melting point, which could not supply the growth of ZnS nanorod arrays in bulk. In stead, a "self-catalytic liquid solid growth" [21] is much more suitable for the explanation of growth mechanism. The redundant Zn droplets appeared on the surface of ZnS nanorod arrays and would gradually absorb sulfur vapor species, which induced the epitaxial growth of these branched structure.

Fig. 3 shows the room temperature Raman spectrum of this kind of ZnS nanostructure excited by 5145 Å line of Ar^+ laser. The spectrum is dominated by the longitudinal optical (LO) phonon peak at 350.0 cm^{-1} and the weaker peak about 270.1 cm^{-1} is associated with the transverse optical (TO) phonon. Compared with the Raman spectrum of bulk hexagonal ZnS with TO ~ 274 cm^{-1} and LO ~ 352 cm^{-1}, the peaks of these first-order LO and TO phonons from our ZnS nanostructure exhibit a shift towards the lower energy. Meanwhile, the Raman lines show substantial broadening. Such phonon softening and line broadening [22] of the Raman peaks could be attributed to quantum confinement effects. It is well known that when the materials structure reduces to nanosize or the lattice distortion increases, the wave-vector selection rule for the first order Raman scattering is relaxed and the photon scattering will not be limited to the centre of the Brillouin zone, the phonon dispersion near the centre of Brillouin zone should be considered as well. Therefore, the combined effects of the relaxation of the wave-vector selection rule and the photon dispersion resulted in the Raman shift, as well as the broadening of the TO and LO peaks. Besides these characteristic peaks, Raman peak about 419.3 cm^{-1} is also observed. The appearance of this phonon feature can be attributed to plasmon-enchanced resonant Raman effect [23].

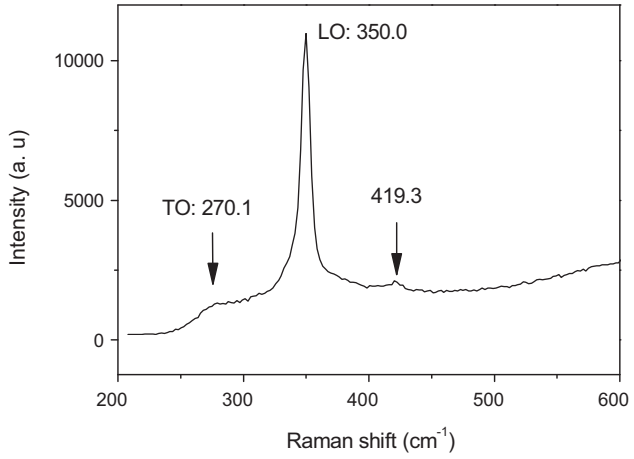

Fig. 3. Raman spectrum of the hierarchical ZnS structure.

Surface wettability of this hierarchical ZnS nanostructured film was studied by CA measurements. When deionized (DI) water droplets about 5 μl were dropped on the surface, it yielded a nearly spherical shape at the microscopic level (shown in Fig. 4(a)). The measured CA was about 153.8°, which was essential difference from ZnS flat surfaces [24] with hydrophilicity. The ZnS superhydrophobic surface exhibited a stable character in air with the CA showing no apparent change for a long time, the water droplet eventually evaporated on the surface. Fig. 4(b) and (c) indicates the consecutive moments that a water droplet slided off the ZnS surface when the inclination angle exceeded 9.1°, which reflects the difference between advancing and receding contact angles. The relatively high CA and low SA gives a further evidence for the super water-repellent properties, indicating that water droplets do not penetrate into the interstices among the hierarchical architecture but rather suspend on it. Theoretically, a thorough understanding of the superhydrophobicity phenomenon can be explained with the Cassie and Baxter equation [25]. For a composite surface, the water CA is influenced significantly by the fractional areas of solid (f_1) versus air pockets (f_2):

$$\cos\theta = f_1 \cos\theta_1 - f_2, \quad (f_1 + f_2 = 1) \tag{1}$$

where θ and θ_1 represent the water contact angles on rough and smooth surfaces, respectively. The well-aligned ZnS nanorod arrays with branched nanowires in thin diameter at the upper layer contributed to the very large fraction of air trapped within the interstices, leading to the greatly increased air/water interface which is essential to superhydrophobic and effectively prevent the penetration of water droplet into the interstices. It is revealed that the hierarchical and branched structure play an important role for preparation of super water-repellent surface. The excellent self-cleaning behavior was demonstrated by scattering natural microparticles from air (the diameter ranging from 1 μm to 40 μm) over the ZnS surface in appropriate density (shown in Fig. 3(d)), then the 'contaminated' sample was fixed on the sample platform of OCA contact angle system, a water droplet was placed on the surface and subsequently tilted the system until it slided off. The photographs of this ZnS nanostructured surface before and after self-cleaning were presented (Fig. 4(d) and (e)), it was clearly seen that the contaminated microparticles were well removed. The interface of the cleaned and uncleaned surface parts is shown in Fig. 3(f).

Fig. 5 shows a selected time sequence of snapshots of a 8 μl water droplet free-falling on the ZnS nanostructured surface from a height of ~15 mm, the water droplet impacts the surface with a velocity corresponding to a dimensionless Weber's index of ~9.2.

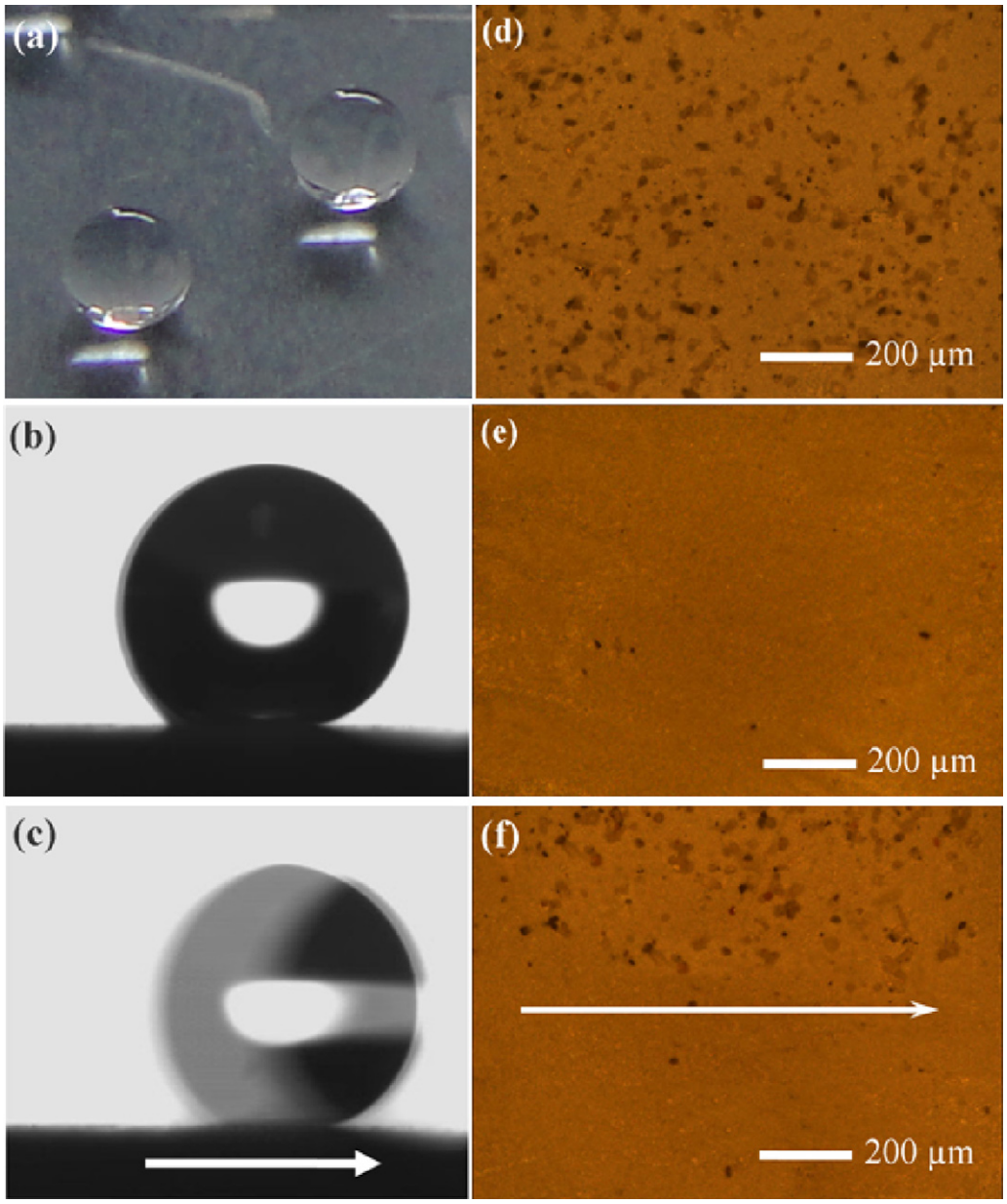

Fig. 4. (a) Photographs of water droplets on the ZnS nanostructured surface and (b and c) the two consecutive moments that a water droplet slided off the ZnS surface when the inclination angle exceeded 9.1°. (d and e) Photographs of the nanostructured surface before and after self-cleaning, the interface of the cleaned and uncleaned surface parts are shown in (f).

Detailed observation discloses that the shape of water droplet changes significantly during the impact process as its kinetic energy transforms into the stored energy induced by surface deformation. In this case, the strong deformation can be attributed to the high Weber's index, signifying the ratio of the arriving kinetic energy to the intrinsic surface energy. We carefully find that the water droplet undergoes two bounces and the bounced heights are estimated to be about 7 mm and 3 mm. The arrowlines in the snapshots represent its movement direction corresponding to different times. When it fell down, it was hardly able to stick the nanostructured surface. This dynamic process further illustrates the superhydrophobic properties.

To investigate the effect of the applied external potential on the droplet stability and wetting behavior, a schematic diagram of the electrowetting setup was shown in Fig. 6(a). A platinum wire was used the counter electrode which was inserted into the

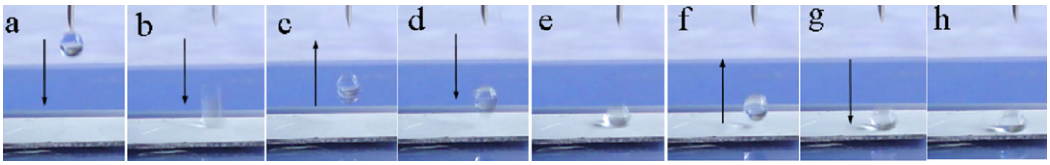

Fig. 5. Selected snapshots of the impact and rebound of a water droplet with the volume ~8 μl.

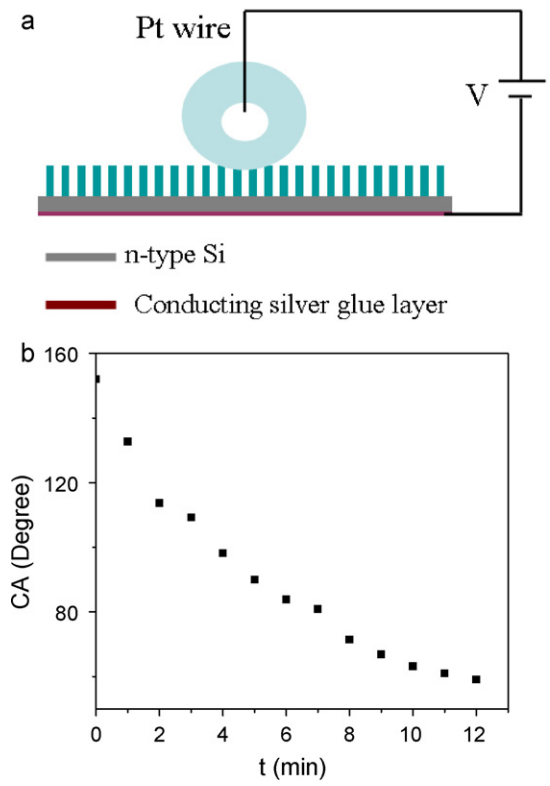

Fig. 6. (a) Schematic illustration of experimental setup for electrowetting, a Pt wire was inserted into the droplet to serve as the top electrode. (b) CA variation versus time for a critical bias of 7.0 V.

water droplet to create electrical contact, the n-type silicon substrate was coated with conducting silver glue layer to insure the resistance on each point of the superhydrophobic surface was equal and it was connected to the negative voltage, varying voltages were applied between the electrodes. First, the initiative voltage was 3.0 V and then with an increase of 0.5 V step by step. We observed the sudden CA changes were not activated unless a threshold voltage was ~7.0 V. Below or equal to this value, the CA changes was less than 5°. When a critical bias raised up to 7.0 V, the water droplet shape dynamically change and a transition from superhydrophobic to hydrophilic state was shown. Fig. 6(b) demonstrates the CA variation versus time in electrowetting process, water CAs become 47.4° and keep nearly constant after 12 min. This observed threshold switching of the water droplet between the Cassie–Baxter state (standing on top of film) and Wenzel state (being penetrated into the interspace) occurred at a threshold voltage of 7.0 V, and it can be ascribed to the accumulation of surface charge reaching a point where it can overcome the high local repulsion force. A comparison of electrowettability for other surfaces made of various nanostructures [8,26–28] revealed that our ZnS product had a lower threshold voltage as well as a larger CA variation. Former study has revealed that a sharp tip was beneficial for activating the transition from superhydrophobic to hydrophilic state [8]. Therefore, the well electrowettability of our ZnS product was believed to be due to the materials feature and the presence of ultra-thin nanowires on the tops.

4. Conclusions

We prepared novel ZnS nanostructures over Au-coated silicon substrate by chemical vapor deposition technique. Measurements showed that this nanostructured surface had an average CA value as high as 153.8° and a relatively low SA about 9.1°. The capability of self-cleaning behavior similar to the lotus effect was demonstrated and super water-repellent properties were dynamically studied by a selected time sequence of snapshots. Wettabilities of surfaces were tested by the application of external voltages. This work possibly actuates the coming researches on water-repellent properties of ZnS nanostructures and induced its application in self-cleaning surface, antifogging or other fields.

Acknowledgments

This work was supported by the Natural Science Foundation of China (grant Nos. 10874115 and 10734020), National Major Basic Research Project of 2010CB933702, Shanghai Nanotechnology Research Project of 0952nm01900, Shanghai Key Basic Research Project of 08JC1411000, and Research fund for the Doctoral Program of Higher Education of Chain.

References

[1] T.L. Sun, L. Feng, X.F. Gao, L. Jiang, Acc. Chem. Res. 38 (2005) 644.
[2] W. Barthlott, C. Neinhuis, Planta 202 (1997) 1.
[3] L. Jiang, X. Yao, H.X. Li, Y.Y. Fu, L. Chen, Q. Meng, W.P. Hu, L. Jiang, Adv. Mater. 21 (2009) 1.
[4] X.F. Gao, L. Jiang, Nature 432 (2004) 36.
[5] L.Y. Gao, M.J. Zheng, M. Zhong, Appl. Phys. Lett. 91 (2007) 013101.
[6] G. Risse, S. Matys, H. Böttcher, Appl. Surf. Sci. 254 (2008) 5994.
[7] F. Xia, H. Ge, Y. Hou, T.L. Sun, L. Chen, G.Z. Zhang, L. Jiang, Adv. Mater. 19 (2007) 2520.
[8] J.L. Campbell, M. Breedon, K. Latham, K. Kalantar-Zadeh, Langmuir 24 (2008) 5091.
[9] S.H. He, M.J. Zheng, L.J. Yao, X.L. Yuan, M. Li, L. Ma, W.Z. Shen, Appl. Surf. Sci. 256 (2010) 2557.
[10] J. Yuan, X.G. Liu, O. Akbulut, J.Q. Hu, S.L. Suib, J. Kong, F. Stellacci, Nat. Nanotechnol. 3 (2008) 332.
[11] S. Minko, M. Müller, M. Motornov, M. Nitschke, K. Grundke, M. Stamm, J. Am. Chem. Soc. 125 (2003) 3896.
[12] N. Verplanck, Y. Coffinier, V. Thomy, R. Boukherroub, Nanoscale Res. Lett. 2 (2007) 577.
[13] W. Sun, S.Y. Zhou, P. Chen, L.M. Peng, Chem. Commun. 603 (2008).
[14] H.Z. Tang, H. Wang, J.H. He, J. Phys. Chem. C 113 (2009) 14220.
[15] N.L. Tarwal, P.S. Patil, Appl. Surf. Sci. 256 (2010) 7451.
[16] W. Yu, P.F. Fang, S.J. Wang, Appl. Surf. Sci. 255 (2009) 5709.
[17] C. Ma, D. Moore, J. Li, Z.L. Wang, Adv. Mater. 15 (2003) 228.
[18] Z.G. Chen, J. Zou, G.Q. Lu, G. Liu, F. Li, H.M. Cheng, Appl. Phys. Lett. 90 (2007) 103117.
[19] Y.C. Zhu, Y. Bando, D.F. Xue, D. Golberg, J. Am. Chem. Soc. 125 (2003) 16196.
[20] M. Wang, G.T. Fei, X.G. Zhu, B. Wu, M.G. Kong, L.D. Zhang, J. Phys. Chem. C 113 (2009) 4335.
[21] S. Biswas, T. Ghoshal, S. Kar, S. Chakrabarti, S. Chaudhuri, Cryst. Growth Des. 8 (2008) 2176.
[22] T.Y. Zhai, Z.J. Gu, H.B. Fu, Y. Ma, J.N. Yao, Cryst. Growth Des. 7 (2007) 1388.
[23] S.M. Scholz, R. Vacassy, L. Lemaire, J. Dutta, H. Hofmann, Appl. Organomet. Chem. 12 (1998) 327.
[24] M.E. Holuszko, J.P. Franzidis, E.V. Manlapig, M.A. Hampton, B.C. Donose, A.V. Nguyen, Miner. Eng. 21 (2008) 958.
[25] A.B.D. Cassie, S. Baxter, Trans. Faraday Soc. 40 (1944) 546.
[26] N. Verplanck, E. Galopin, J.-C. Camart, V. Thomy, Y. Coffinier, R. Boukherroub, Nano Lett. 7 (2007) 813.
[27] T. Krupenkin, J.A. Taylor, P. Kolodner, M. Hodes, Bell Labs Tech. J. 10 (2005) 161.
[28] Z. Wang, Y. Ou, T.-M. Lu, N. Koratkar, J. Phys. Chem. B 111 (2007) 4296.